Higher Martian atmospheric temperatures at all altitudes lead to enhanced D/H fractionation and water loss

E. M. Cangi[1,2], M. S. Chaffin[1], J. Deighan[1]

[1]Laboratory for Atmospheric and Space Physics
[2]University of Colorado Boulder
[1]3665 Discovery Dr, Boulder, CO 80303
[2]Boulder, CO

Key Points:

- The fractionation factor f ranges from 10^{-5} to 10^{-1} for thermal escape only, and 0.03 to 0.1 for thermal + non-thermal escape.
- f is insensitive to atmospheric temperature at the surface, but depends strongly on exobase and tropopause temperatures.
- Using our results for f, we calculate total water lost from Mars to be between 66-123 m GEL, which is likely a lower bound.

Corresponding author: Eryn Cangi, eryn.cangi@colorado.edu

Abstract

Much of the water that once flowed on the surface of Mars was lost to space long ago, and the total amount lost remains unknown. Clues to the amount lost can be found by studying hydrogen (H) and its isotope deuterium (D), both of which are produced when atmospheric water molecules H_2O and HDO dissociate. The freed H and D atoms then escape to space at different rates due to their different masses, leaving an enhanced D/H ratio. The rate of change of D/H is referred to as the fractionation factor f. Both the D/H ratio and f are necessary to estimate water loss; thus, if we can constrain the range of f, we will be able to estimate water loss more accurately. In this study, we use a 1D photochemical model of the Martian atmosphere to determine how f depends on assumed temperature and water vapor profiles. We find that for most Martian atmospheric conditions, f varies between 10^{-1} and 10^{-5}; for the standard Martian atmosphere, $f = 0.002$ for thermal escape processes, and $f \approxeq 0.06$ when both thermal and non-thermal escape are considered. Using these results, we estimate that Mars has lost at minimum 66-123 m GEL of water. Our results demonstrate that the value of f is almost completely controlled by the amount of non-thermal escape of D, and that photochemical modeling studies that include fractionation must thus model both neutral and ion processes throughout the atmosphere.

Plain Language Summary

Much of the water that once flowed on the surface of Mars was lost to space long ago, and the total amount lost remains unknown. Clues can be found by studying the two types of water: the familiar H_2O, and HDO, a heavier version of water. When water molecules break apart in the atmosphere, they release hydrogen (H) and its heavier twin deuterium (D), which escape to space at different rates, removing water from Mars. The difference in escape efficiency between H and D is called the fractionation factor f. The goal of this study is two-fold: to understand how f varies with different atmospheric conditions and the processes that control it, and to use that information to estimate water loss from Mars. To do this, we model the atmospheric chemistry of Mars, testing different atmospheric temperatures and water vapor content to understand how they affect f. Using the results for f, we calculate that Mars has lost enough water to cover the whole planet in a layer between 66-123 m deep, in agreement with other photochemical modeling studies, but still short of geological estimates.

1 The D/H Fractionation Factor and Loss of Martian Water to Space

The surface of Mars is marked with ample evidence of its wetter past. Today, water on Mars exists only in the polar caps, subsurface ice, and atmosphere, but geomorphological and geochemical evidence points to significant alteration of the surface by liquid water. The presence of compounds like jarosite and hematite indicate past pooling and evaporation (Squyres et al., 2004; Klingelhöfer et al., 2004), while substantial evidence of hydrated silicates supports the theory that ancient river deltas, lakebeds, catastrophic flood channels, and dendritic valley networks were formed by water (M. H. Carr & Head, 2010; Ehlmann & Edwards, 2014, and references therein). Because the contemporary Martian climate is too cold and too low-pressure to support liquid water on the surface, all this evidence means that Mars must have had both a thicker and warmer atmosphere, and therefore a stronger greenhouse effect. Identifying the greenhouse gas responsible is the topic of ongoing studies (Ramirez et al., 2014; Wordsworth et al., 2017). Regardless, the Mars science community generally agrees that a significant amount of the once-thick Martian atmosphere has escaped to space over time. Most of this escape occurs in the form of thermal escape of H, in which a fraction of H atoms are hot enough that their velocity exceeds the escape velocity. Because H is primarily found in water

on Mars, integrated atmospheric escape has effectively desiccated the planet (Jakosky et al., 2018).

A significant indicator of this loss of water to space is the elevated D (deuterium, ^{2}H or D) to H (hydrogen, ^{1}H) ratio, which we will abbreviate as R_{dh}. On Mars, water (either as H_2O or HDO) is the primary reservoir of both H and D. When we talk about the D/H ratio, we are thus usually referring to the D/H ratio as measured in water:

$$R_{dh} = \frac{\text{D in HDO}}{\text{H from HDO} + \text{H from } H_2O} = \frac{[HDO]}{[HDO] + 2[H_2O]} \approxeq \frac{[HDO]}{2[H_2O]} \tag{1}$$

Here, $[X]$ represents a molecule's abundance; H sourced from HDO is negligible compared to H sourced from H_2O. This ratio evolves according to differential escape of D and H; D, being twice as massive as H, is less likely to escape. This difference can be characterized as a relative efficiency, the fractionation factor f:

$$f = \frac{\phi_D/\phi_H}{[HDO]_0/2[H_2O]_0} = \frac{\phi_D/\phi_H}{R_{dh,0}} \tag{2}$$

where ϕ represents outgoing fluxes to space, and the 0 subscript specifies the near-surface atmospheric reservoir, which approximates the total amount in the atmosphere. As it represents efficiency of D escape, f takes on values between 0 and 1. When f is 0, D is completely retained on the planet, and cumulative water loss must have been lower than for $f \neq 0$. When $f = 1$, the *ratio* of escaping to retained atoms is the same for both D and H, and there is no mass effect on the escape rates. In this scenario, no amount of escape is sufficient to change the D/H ratio in any species. In practice, f is somewhere in between these extremes.

Over geologic time, this fractionation manifests as an enhancement of the D/H ratio compared to the Earth ratio of 1.6×10^{-4} (Yung et al., 1988), called SMOW (for the measured source, Standard Mean Ocean Water). A planet's D/H ratio is often quoted as a multiple of the Earth value. At present, multiple measurements put the global mean R_{dh} on Mars between 4 and 6 × SMOW (Owen et al., 1988; Bjoraker et al., 1989; V. Krasnopolsky et al., 1997; Encrenaz et al., 2018; Vandaele et al., 2019), with some variations occurring on local spatial and temporal scales (Villanueva et al., 2015; Clarke et al., 2017; Encrenaz et al., 2018; Clarke et al., 2019; Villanueva et al., 2019). This is most commonly interpreted as evidence for significant escape to space of H.

Current estimates of the Martian water inventory, R_{dh}, and f are used with the Rayleigh distillation equation to estimate the integrated amount of water lost from Mars. The Rayleigh distillation equation for H on Mars is (Yung & DeMore, 1998):

$$R_{dh}(t) = R_{dh}(t=0)\left(\frac{[H](0)}{[H](t)}\right)^{1-f} \tag{3}$$

Where $t = 0$ can be arbitrarily chosen. Because we use R_{dh}, [H] is a proxy for total water W (W = [H_2O] + [HDO]). Then $W(0)$, the total water on Mars at some point in the past $t = 0$, is the sum of the water budget at time t and the total water lost: $W(0) = W(t) + W_{\text{lost}}$. Substituting W for [H] and rearranging equation 3, we obtain an expression for water lost from Mars:

$$W_{lost} = W(t)\left(\left(\frac{R_{dh}(t)}{R_{dh}(0)}\right)^{1/(1-f)} - 1\right) \tag{4}$$

Most of the inputs to Equation 4 are well-described. The current D/H ratio of exchangeable water (the atmosphere, seasonal polar caps, ground ice, and water adsorbed in the regolith), $R_{dh}(t)$, is 4−6× SMOW as mentioned (we use 5.5 in this study). $R_{dh}(0)$ is usually taken to be that at Mars' formation, when it would have been similar to the Earth's D/H ratio (Geiss & Reeves, 1981); R_{dh} at other points in time can be obtained from analysis of Martian surface material. These studies are limited; meteorite samples (Usui et al., 2012) provide some data, and in-situ analysis at Mars more (Mahaffy et al., 2015). The current water inventory in exchangeable reservoirs, $W(t)$, is estimated to be between 20-30 m GEL (global equivalent layer), the depth of water if the entire exchangeable inventory were rained onto the surface (Lasue et al., 2013; Villanueva et al., 2015; M. Carr & Head, 2019).

Prior studies produced best estimates of the fractionation factor f, but its range of values under all plausible scenarios has been largely unexplored. Yung et al. (1988) used a 1D photochemical model to calculate a first value of $f = 0.32$ which has been frequently referenced in the years since. They explored the effects of certain chemical reactions on f, but did not test other parameters. V. A. Krasnopolsky and Mumma (1998) obtained $f = 0.02$ by combining Hubble Space Telescope observations with a radiative transfer and 1D photochemical model. Later, V. Krasnopolsky (2000) followed up with another study that tested the effects of two different models of eddy diffusion, finding values of $f = 0.135$ and $f = 0.016$. Two years later, V. A. Krasnopolsky (2002) released another study that found 3 values for f, depending on whether the solar cycle was at minimum ($f = 0.055$), maximum ($f = 0.167$), or mean ($f = 0.082$), represented in the model by variation of the exobase temperature and non-thermal escape flux. Our goal is to advance this body of work by performing the first systematic parameter-space study of the fractionation factor with respect to the assumed atmospheric temperature and water vapor profiles.

2 Building Our 1D Photochemical Model

To best capture the mean behavior of the Martian atmosphere over long time scales, we use a 1D photochemical model, extended from the original developed by Chaffin et al. (2017) to include D chemistry. The model uses standard photochemical techniques described in other studies (V. Krasnopolsky, 1993; Nair et al., 1994; Chaffin et al., 2017), with the addition of the D-bearing species D, HD, HDO, OD, HDO_2, DO_2, and DOCO. The chemical reactions for D-bearing species came from several sources, including past papers (Yung et al., 1988; Yung et al., 1989; Cazaux et al., 2010; Deighan, 2012), NASA publications (Sander et al., 2011), and online databases (Manion et al., 2015; Wakelam & Gratier, 2019; McElroy et al., 2013). The full list of chemical reactions and reaction rates, as well as information on photochemical cross sections and diffusion coefficients, is given in the Supporting Information. Photodissociation is driven by solar UV irradiation data from SORCE/SOLSTICE and TIMED/SEE (Woods et al., 2019), appropriate for solar mean conditions and scaled to Mars' orbit. For our primary input, we construct temperature and water vapor profiles designed to represent end-member states of the atmosphere, such that we fully constrain the range of plausible fractionation factor values.

A run of the model consists of the following steps: (1) loading the temperature and water vapor profiles, (2) establishing an initial condition of species number densities, (3) establishing boundary conditions (available in Table S3), (4) stepping forward over 10 million years of simulation time until the atmosphere reaches chemical equilibrium, which is achieved when the combined escape flux of atomic H and D ($\phi_H + \phi_D$) is twice that of the escape flux of atomic O (ϕ_O). The model output comprises species number densities by altitude. By multiplying the H and D densities by the their thermal effusion velocities (Hunten, 1973), we can calculate the escape fluxes of H and D, ϕ_H and ϕ_D. These fluxes are then used to calculate f according to equation 2.

A limitation of our model is that we do not include a full ionosphere. Instead, we approximate it by including a static profile of CO_2^+ (Matta et al., 2013), enabling the primary H-producing ion reaction in the Martian atmosphere; a similar tactic was used by Yung et al. (1988). Without a full ionosphere, we are not able to model non-thermal escape of H or D, as most non-thermal processes depend on ions. In an effort to estimate the relative importance of non-thermal processes to the fractionation factor, we estimate non-thermal effusion velocities for our model conditions, scaled from V. A. Krasnopolsky (2010), described further in Section 3.

2.1 Reproductions of Past Studies

Before proceeding with our study, we attempted to reproduce the results by Yung et al. (1988) and V. A. Krasnopolsky (2002). Their original results and our reproductions are shown in Figure S3. We achieved very good agreement with the results by Yung et al. (1988) ($f = 0.26$ versus their $f = 0.32$), with the small difference being due to an inability to reproduce the exact same photodissociation rates due to self-consistent calculation. Our results for f were consistent with V. A. Krasnopolsky (2002) for solar maximum, but comparatively low for solar mean and minimum. We expect that this is because their model includes an ionosphere, allowing them to model non-thermal escape of D. To account for this, we added their results for non-thermal escape of D to our results for thermal escape, resulting in a slight *overestimate* of f for all solar states. This change was a first hint at the importance of non-thermal escape to f. The remaining discrepancy is due to other significant model differences; for example, their model atmosphere has its lower bound at 80 km, while ours is at the surface.

2.2 Model input: Temperature and Water Vapor Profiles

Our temperature and water vapor vertical profiles remain fixed for the duration of a simulation. This allows us to examine the mean behavior of the atmosphere over long time scales.

2.2.1 Temperature Profiles

The piecewise temperature profile is constrained by the temperature at the surface (T_{surf}), mesosphere (T_{tropo}), and exobase (T_{exo}):

$$T = \begin{cases} T_{\mathrm{exo}} - (T_{\mathrm{exo}} - T_{\mathrm{tropo}}) \exp\left(-\frac{(z-120)^2)}{(8T_{\mathrm{exo}})}\right) & z > 120 \text{ km} \\ T_{\mathrm{tropo}} & z_t < z < 120 \\ T_{\mathrm{surf}} + \Gamma z & z < z_t \end{cases} \tag{5}$$

where 120 km is the altitude of the mesopause, z_{t} is the altitude of the tropopause and Γ is the lapse rate. Constraining the temperature at these three points requires either Γ or z_t to vary; if they are both fixed, the profile will be over-constrained and discontinuous. We allow z_t to vary because it does vary in reality; exactly what sets its altitude is less well defined than the dynamics of gas and dust, on which Γ depends. We use $\Gamma = -1.4$ K/km, which is slightly lower than the standard dry adiabatic lapse rate due to warming effects from suspended dust (Zahnle et al., 2008).

For the first part of the study, we constructed a standard temperature profile representing current conditions on Mars, as well as 6 alternate profiles intended to represent plausible climate extremes driven by changing planetary obliquity throughout the last ∼10 million years of Mars' history, the maximum time over which evolution of the obliquity can be analytically predicted. (On longer time scales, the obliquity evolves chaotically, making precise definition of climate parameters impossible (Laskar et al., 2004).) We used the Mars Climate Database (MCD) (Millour & Forget, 2018) to obtain values

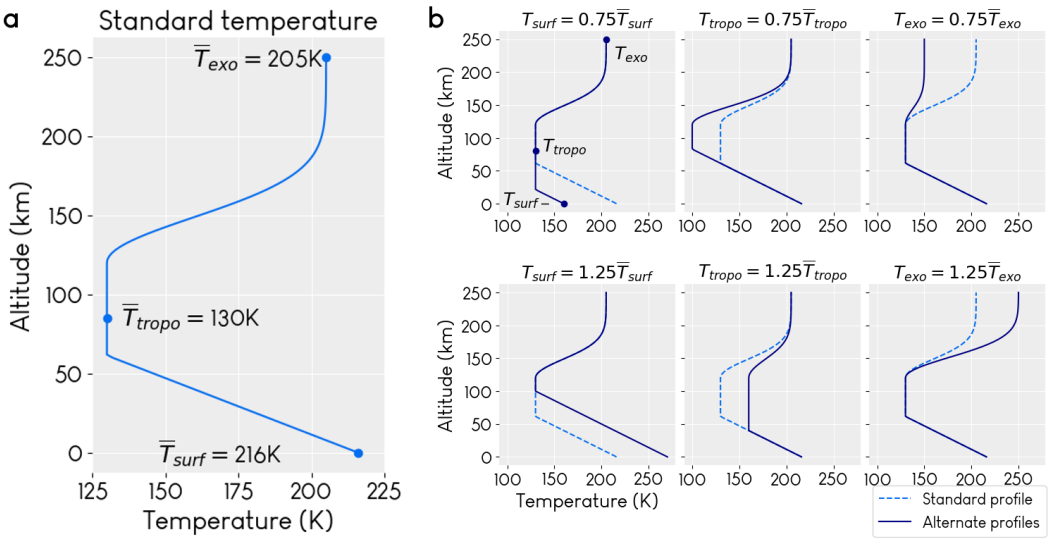

Figure 1. a) Our standard temperature profile used in the model, and b) alternate temperature profiles representing plausible climate extrema due to obliquity variations. Profiles are created by modifying the standard temperatures $\overline{T}_{surf}$, $\overline{T}_{tropo}$, or $\overline{T}_{exo}$ by ±25%. We do not consider effects of CO_2 condensation for cold temperatures, although this is likely to be important in reality. These profiles, along with the standard profile, are used to obtain the results in Figure 4. Table S4 gives specific values for T_{surf}, T_{tropo}. T_{exo}.

for $T_{\rm surf}$ (z = 0), $T_{\rm tropo}$ (z = 100 km), and $T_{\rm exo}$ (z = 250 km) for different times of sol (local times 03:00, 09:00, 15:00, 21:00), Mars latitude (90°N, 45°N, 0°, 45°S, 90°S), and L_s (90° and 270°). The mean temperatures across each of these parameters were then compared with data from multiple missions to ensure consistency. The surface temperature was compared with the Curiosity Rover (Vasavada et al., 2016; Audouard et al., 2016; Savijärvi et al., 2019), Mars Global Surveyor Thermal Emission Spectrometer (TES) (Smith, 2004), and the Spirit/Opportunity Rovers' Mini-TES (Smith et al., 2006); the exobase temperature was compared with MAVEN data from multiple instruments (Bougher et al., 2017; Stone et al., 2018; Thiemann et al., 2018). The mean temperatures formed the standard profile, shown in Figure 1a. The 6 alternate profiles are shown in Figure 1b. For each, we either increased or decreased one of $T_{\rm surf}$, $T_{\rm tropo}$, or $T_{\rm exo}$ by 25% of the standard value. This variation covers most values observed by current missions, as well as temperatures calculated (Wordsworth et al., 2015) for obliquities of ∼25-45°predicted for the last 10 million years (Laskar et al., 2004). A table with the control temperatures for each profile is available in the Supporting Information. Together, the standard and alternate temperature profiles represent end-member cases for the Martian atmosphere.

In addition to these select profiles, we also created a larger set of temperature profiles with finer variation in each of $T_{\rm surf}$, $T_{\rm tropo}$, or $T_{\rm exo}$ to examine the details of how each parameter affects f. The full array of temperature profiles is shown in Figure 2.

2.2.2 Water Profiles

H_2O and HDO profiles used in the model are shown in Figure 3. We require that the profiles have total water content (H_2O + HDO) equal to 1, 10, 25, 50, or 100 pr μm (precipitable micrometers), with H_2O making up most of the share. Higher concentrations of water vapor would require a supersaturated atmosphere; while there is obser-

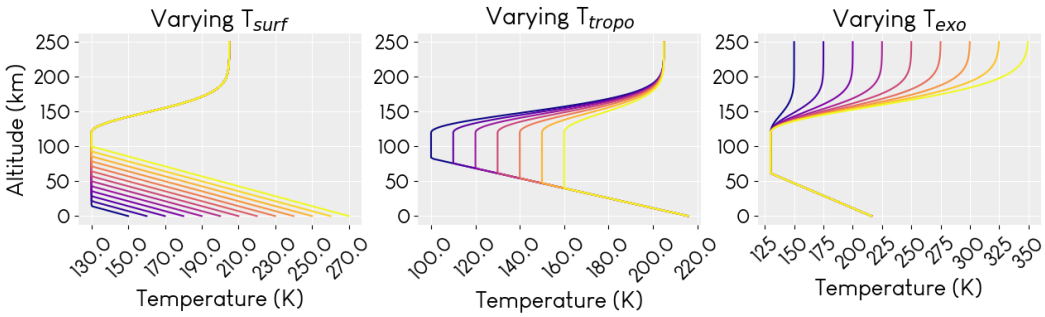

Figure 2. The full range of temperature profiles tested. Each panel represents a set of profiles in which one of the specifiable temperatures was varied. Results from the simulations using these profiles are shown in Figure 5. Each color represents a different profile.

vational evidence of supersaturation at upper altitudes in specific cases, (Maltagliati, 2011; Fedorova et al., 2020), our model does not include it. We use the 10 pr μm profile to represent the long-term standard atmosphere, a value in agreement with observations (Lammer et al., 2003; Smith, 2004), although more recent observations (Heavens et al., 2018; Vandaele et al., 2019) and modeling (Shaposhnikov et al., 2019) suggest that local water vapor concentrations can reach higher values, up to 150 pr μm, on very short timescales, particularly during dust storms. We assume that the lower atmosphere is well-mixed, such that the water vapor mixing ratio is constant. At the hygropause, usually between 25 and 50 km (V. Krasnopolsky, 2000; Heavens et al., 2018), water begins to condense, and its mixing ratio follows the saturation vapor pressure curve until it becomes negligible in the upper atmosphere (Heavens et al., 2018). Although HDO preferentially condenses compared to H_2O (Montmessin et al., 2005), it never approaches saturation in our model atmosphere, allowing us to use the same empirical saturation vapor pressure equation (Marti & Mauersberger, 1993) for both H_2O and HDO. This is helpful, as no empirical equation for HDO exists, and the enthalpies of HDO under Mars-like conditions are very sparsely studied.

Although observations (Villanueva et al., 2015) and modeling (Fouchet & Lellouch, 1999; Bertaux & Montmessin, 2001) have shown that atmospheric D/H varies between 1-10× SMOW depending on the species it is measured in, altitude, and latitude/longitude, we tested these variations and determined that they had no effect on our results. We therefore multiply the initial profiles of H-bearing species by the D/H ratio of 5.5× SMOW to create the D-bearing profiles. The number densities of H_2O and HDO remain fixed during the simulation to represent the standard water abundance, though they are used to calculate chemical reaction rates.

3 Results: Non-thermal Escape Critical to Understanding the Fractionation Factor

Figure 4 shows the range of the fractionation factor as a function of each temperature and water vapor parameter, using the temperature profiles in Figure 1 and the water vapor profiles in Figure 3–that is, the standard profiles and the plausible climate extrema profiles. Results for the broad range of temperatures shown in Figure 2 are discussed in Section 3.1.

For thermal escape only, we find that the fractionation factor is 1-3 orders of magnitude lower than the original value by Yung et al. (1988). The primary reason for this difference is the exobase temperature (they use 364 K, we use a maximum of 250 K). Ad-

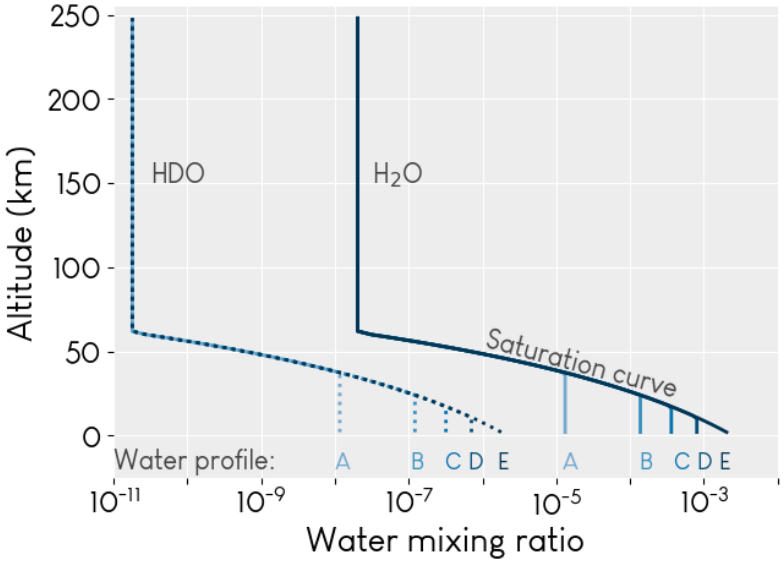

Figure 3. Water vapor profiles used in our model. A single profile, e.g. A, comprises both H_2O (solid lines) and HDO (dotted). Profiles are constrained by requiring that [H_2O]+[HDO] = 1 pr μm (profile A), 10 (B), 25 (C), 50 (D), or 100 (E) and that the HDO profile is equal to 5.5 × SMOW × the H_2O profile. Profiles differ in the well-mixed lower atmosphere and are the same once they reach the saturation vapor pressure curve. Water vapor in the mesosphere and upper atmosphere is negligible on average over long time scales, like those we model, although it may change on short time scales (see text). Profile B (10 pr μm) is used for our standard atmosphere.

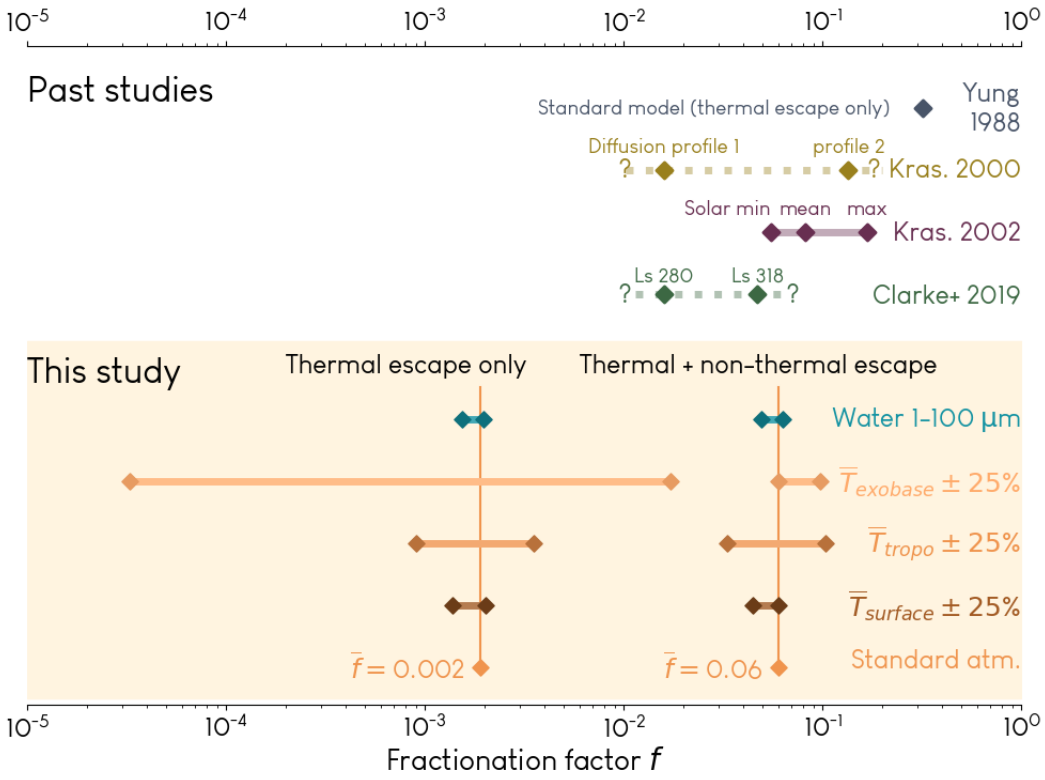

Figure 4. Results for the fractionation factor from this study (lower panel) and in past studies (upper panel). Bars represent the approximate range. Dotted lines with question marks indicate a study where the cases chosen did not necessarily represent end-member cases, so the true range is uncertain. Details of the dependence of f on temperatures and water vapor (orange and blue bars in lower panel) are shown in Figures 5 and 7. A numerical table of our results is available in Table S5.

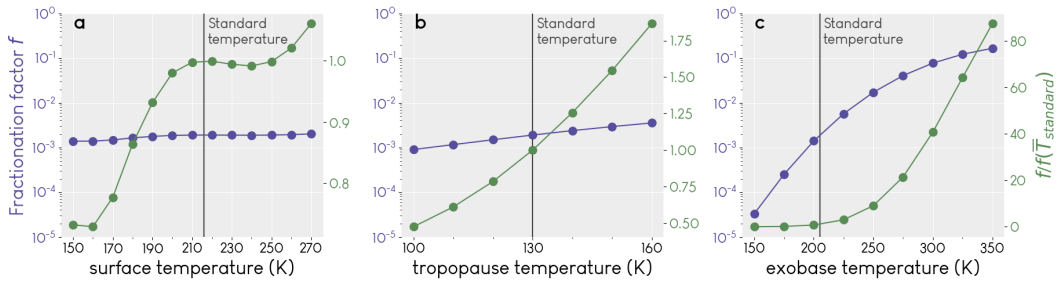

Figure 5. Dependence of the fractionation factor f on changes in the surface, tropopause, and exobase temperatures. The standard value of each is marked by a black vertical line. The left (purple) axis shows the value of f, while the right (green) axis shows the relative change of f with respect to that calculated for the standard temperature.

ditionally, they allow their model to self-consistently solve for water vapor number density above 80 km, while our entire profile is fixed. Updates in chemical and photochemical reaction rates over the last three decades are the last key difference. Details of the dependence of f on each parameter are discussed in sections 3.1 and 3.2.

Because our model does not include an ionosphere, we do not model the effects of non-thermal escape processes, including sputtering, ion outflow, photochemical escape, ion pickup, or bulk ion escape. In order to approximate the effect of non-thermal escape, we calculated the ratio of thermal (v_t) to non-thermal (v_{nt}) effusion velocities for the H, H_2, D, and HD species in the model used by V. A. Krasnopolsky (2002). We then used our model results for v_t and the ratio to estimate non-thermal effusion velocities for our modeled temperatures. This allowed us to estimate the role that non-thermal escape plays in setting f. The resulting values of f are consistent with V. Krasnopolsky (2000) and (V. A. Krasnopolsky, 2002), as well as more recent observations using MAVEN/IUVS (Clarke et al., 2019). Notably, our highest value of f is approximately a factor of 3 larger than the lowest, in agreement with V. A. Krasnopolsky (2002).

3.1 Fractionation Factor Strongly Controlled by Exobase Temperature in Thermal Escape

Figure 5 shows in detail how f varies with each temperature parameter. In these cases, we only report results for modeled thermal escape, in order to focus on what we can learn about f from our model, and refrain from drawing any strong conclusions about what effects may be introduced by non-thermal escape before we can fully model it.

Though the effect is small, f increases as a function of surface and tropopause temperature. The cause of this increase is revealed by examining how the absolute abundances of H, D, H_2, HD, and the escape fluxes ϕ_D and ϕ_H vary with each temperature parameter; this information is shown in Figure 6. To visualize this, we calculate the ratio of these abundances and fluxes in a given simulation (e.g., $T_{surf} = 190$ K) to the standard atmosphere simulation ($T_{surf} = 216$ K). The standard atmosphere case thus has a ratio of 1, and any simulation in which a species abundance or flux increases (decreases) relative to the standard atmosphere will have a ratio greater than (less than) 1. As a function of both surface and tropopause temperature, ϕ_D most closely tracks the abundance of atomic D at the exobase. f depends directly on ϕ_D, inversely on ϕ_H, and inversely on $R_{dh,0}$. Because $R_{dh,0}$ never changes, and because ϕ_H is consistent across all temperatures, the increase of f with surface or tropopause temperature is due to a preferential increase in D at the exobase due to chemical or photochemical reactions. The increase is not likely due to transport, as D is less able to diffuse upward.

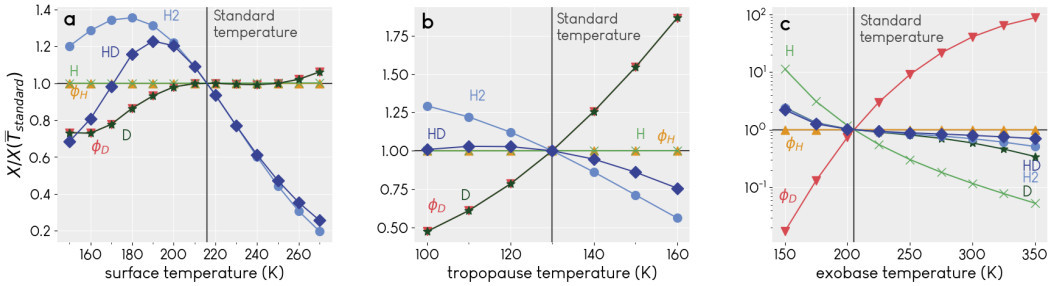

Figure 6. Change in exobase abundances of H- and D-bearing species or escape fluxes (ϕ) as a function of temperature for thermal escape only. ϕ_H includes loss from H, H_2, and HD, while ϕ_D includes loss via D and HD. In (a) and (b), ϕ_D (and thus f in Figure 5a and (b)) closely tracks the abundance of atomic D. In panel (c), changes in the abundance of H, D, H_2 and HD are caused by both escape to space and supply by diffusion from below. Because of D's low abundance, ϕ_D responds more strongly to temperature forcing than H. Note the linear y-scale in panels a and b and the log scale in panel (c).

In contrast, the exobase temperature has a far greater effect on the value of f, with values ranging from 10^{-5} to 10^{-1}. This is unsurprising, as f directly depends on the escape fluxes ϕ_D, ϕ_H at the exobase. The escape flux is the product of the species X number density n_X and the escape velocity, v_{esc}. Because the thermal population of H is assumed to be Maxwellian, we take the escape velocity to be the effusion velocity, which directly depends on the temperature of the exobase. D is preferentially affected compared to H; in Figure 6c, a much larger decrease in the abundance of H at the exobase compared to D is revealed, leading to a relative increase in ϕ_D compared to ϕ_H and an increase of f. This is likely due to greater diffusive separation of H in the heterosphere at low temperature.

3.2 Fractionation Factor Depends Weakly on Water Vapor Column Abundance

The fractionation factor as a function of total water vapor is shown in Figure 7a, and the comparison of abundances and fluxes of H- and D-bearing species in Figure 7b. As in the previous section, the increase of f with additional water vapor is correlated with an increased abundance of D at the exobase, but also HD. The total water vapor has little effect on f, likely because the absolute abundance of water changes neither the D/H ratio in water or the processes by which it is fractionated. The small variation with respect to water vapor thus reflects the influence of minor differences in H_2O and HDO chemical and photochemical reactions. In order to more fully characterize the effects of water vapor on the fractionation factor, the model will have to be modified to allow variable water vapor profiles.

3.3 Mapping Fractionation Factor Results to Integrated Water Loss

We can determine the magnitude of water loss on Mars by using our results for f as input to Equation 4. These results are shown in Figure 8. In order to use Equation 4 to plot past water loss, we must set values for the current water inventory $W(t)$, the current D/H ratio $R_{dh}(t)$, and the ancient Martian D/H ratio, $R_{dh}(0)$.

For $W(t)$, we use the range 20-30 m GEL to encompass the range of observations of the current exchangeable water budget of Mars (Villanueva et al., 2015; Lasue et al.,

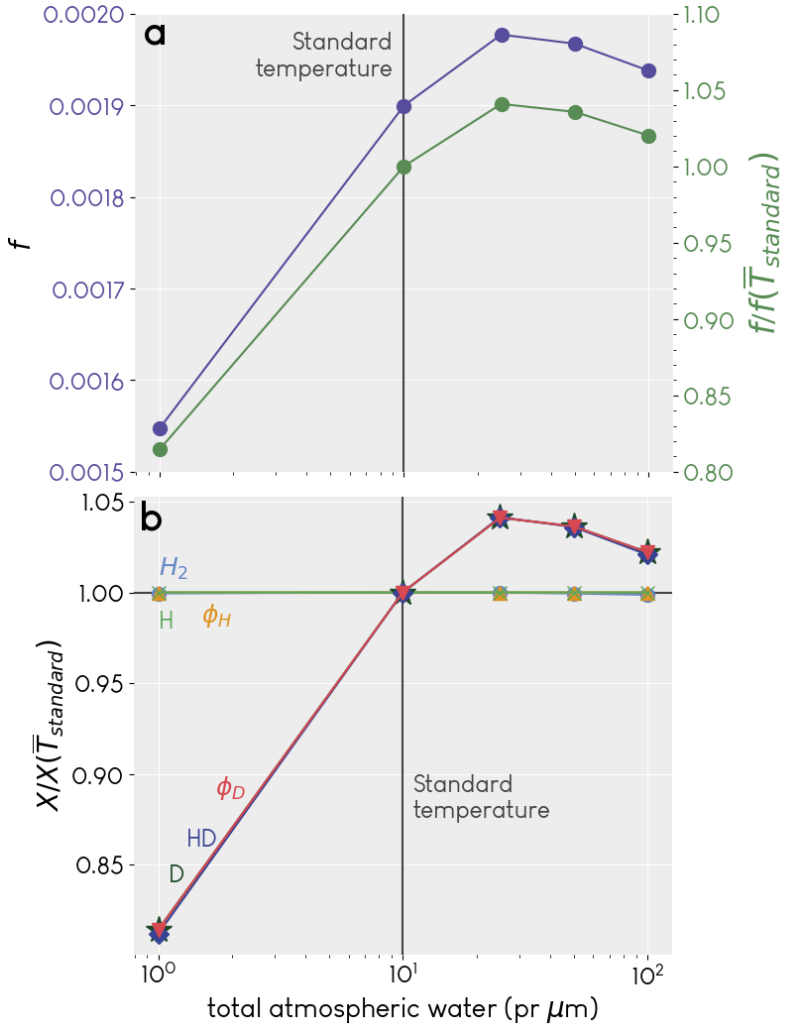

Figure 7. a) Fractionation factor as a function of water vapor column abundance, shown for concentrations of 1, 10, 25, 50, and 100 pr μm, for thermal escape only. b) Same as Figure 6, but as a function of water vapor. Here, ϕ_D and f track the abundances of both D and HD.

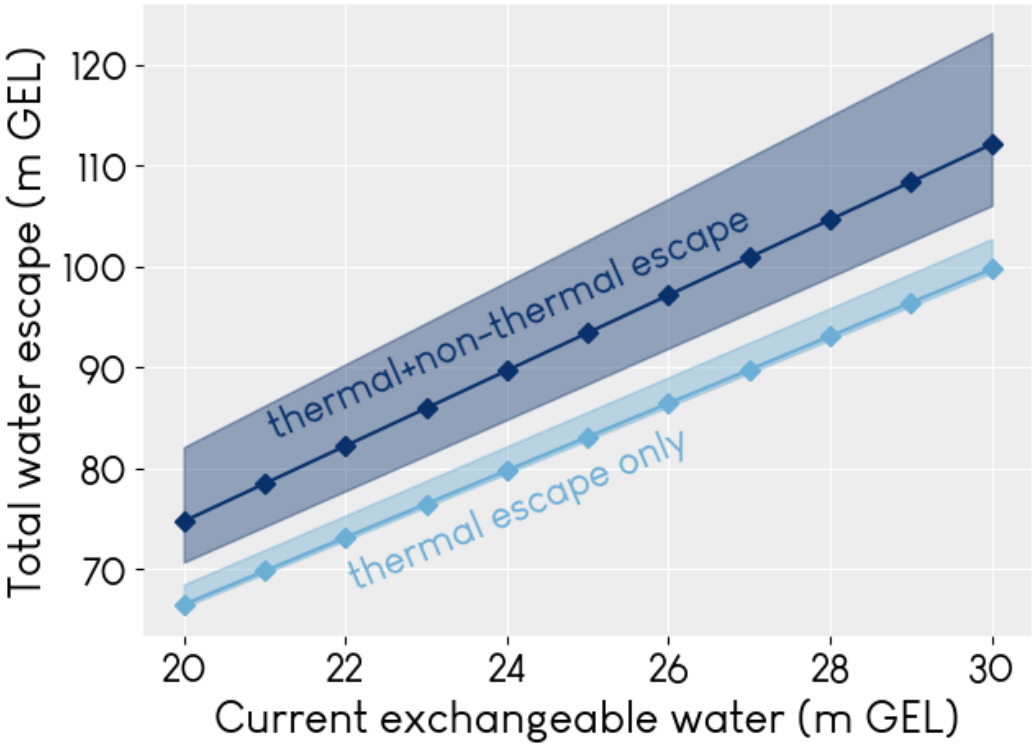

Figure 8. Water lost from Mars as a function of the current exchangeable water budget and the fractionation factor, calculated using Equation 4, where the slope of each line is $(R_{dh}(t)/R_{dh}(0))^{1/(1-f)} - 1$. We use $R_{dh}(t) = 5.5\times$ SMOW, $R_{dh}(0) = 1.275\times$ SMOW (Villanueva et al., 2015). For thermal escape only, we use our result for the standard atmosphere, $f = 0.002$; for the thermal and non-thermal case, $f = 0.06$. The shaded regions represent the extrema of water loss, calculated for the extrema of f of each escape type from our results. The lower bound for thermal escape is close to that of the standard case because water loss is insensitive to f for $f < 0.01$.

2013). Exchangeable water is water that is able to move between surface deposits and the atmosphere; its D/H ratio increases due to escape to space. Non-exchangeable water, being unaffected by escape to space, would have its original D/H value.

For $R_{dh}(0)$, we follow Villanueva et al. (2015) and use 1.275 × SMOW, in agreement with the measurement of D/H in the 4.5 billion year old melt inclusions in the Martian meteorite Yamato 980459 (Usui et al., 2012). Finally, we use 5.5 × SMOW for $R_{dh}(t)$.

Using these values, we calculate the water lost over 4.5 billion years (Ga) to be between about 66 and 123 m GEL, depending on escape type and value of f. We compare these results with other estimates in the literature in the next section.

4 Discussion

Because the fractionation factor depends directly on the escape fluxes ϕ_D and ϕ_H, it is reasonable that the exobase temperature would most strongly affect f. Disturbances in the lower atmosphere that may otherwise affect f will be generally depleted in amplitude by the time they propagate to the upper atmosphere. A larger f at higher exobase temperatures also makes sense in the context of past work; the Mariner missions measured the exobase temperature to be 350 ± 100 K (Anderson & Hord, 1971), and Yung et al. (1988) used $T_{exo} = 364$ K to obtain $f = 0.32$ for thermal escape only. However, these original Mariner measurements were highly uncertain; more recent data (discussed previously) indicate that T_{exo} during solar mean and minimum is cold enough that f for thermal escape is substantially smaller, and that non-thermal escape of D is critical to an accurate calculation of f.

The relationship of ϕ_D to the abundances of atomic D and HD is not immediately obvious. In Figure 6a and b, ϕ_D most closely tracks the abundance of atomic D at the exobase because it is much more abundant than HD. In all of the simulations represented in these panels, the exobase temperature is 205K, a value too low for escape of HD to contribute significantly to D loss. Only at high exobase temperatures (Figure 6c) or high concentrations of water near the exobase (Figure 7b) does the HD line get closer to the ϕ_D line, indicating HD is abundant enough to contribute more to D loss. In general, in Figures 6 and 7b, the more closely the ϕ_D line tracks either the D or HD lines, the more abundant that species is at the exobase. A higher abundance leads to a greater contribution to escape; in most cases, loss of D (H) via the atomic form dominates, but at high exobase temperatures, loss via the molecular form HD (H_2) can reach higher values, up to 5% (20%), as shown in Figure S4.

A comparison of our results for water loss to those of other similar studies is shown in Figure 11. Overall, our results agree reasonably well with these other studies. Our results are a little lower than those by Villanueva et al. (2015), who assume a higher atmospheric D/H ratio (7-8 × SMOW), and a little higher than Lammer et al. (2003), who use both a higher assumed D/H ratio for early Mars (1.2-2.6 × SMOW) and a lower estimate of the current exchangeable water (3.3-15 m GEL). The original study by Yung et al. (1988) is an outlier in this case because they were attempting to determine both the current water inventory and the amount lost, and did not have the benefit of the many Mars missions and observations that we have today.

Our results for water loss also bring up an important point with regard to escape rates. It is common when estimating water loss on Mars to assume that the escape fluxes ϕ_H and ϕ_D are constant and that the water inventory decreases linearly with time. This is an often necessary but imperfect assumption due to the many unknowns involved, including historical rates of atmospheric escape and their evolution in light of Mars' chaotically evolving obliquity. Assuming linear loss with time (and neglecting ϕ_D, which is far slower than ϕ_H) gives $\phi_H = W_{lost}/t$, where t is the time over which the water has been lost. Using our results for water loss, even the smallest amount lost (about 60 m

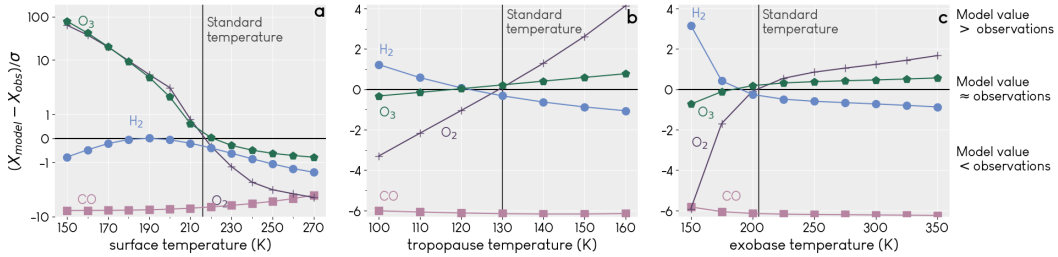

Figure 9. Comparison of model output values to measured values as a means of determining appropriateness of our temperature assumptions. See text for measurement citations. O_3 is measured in μm-atm. O_2 and CO are measured as the mixing ratio at the surface. H_2 is measured with the total abundance in ppm in the lower atmosphere (0-80 km). The y-axis is the difference between model output and measurement, weighted by the uncertainty in the measurement; the closer a point is to the 0 line, the more similar the model output and measurement.

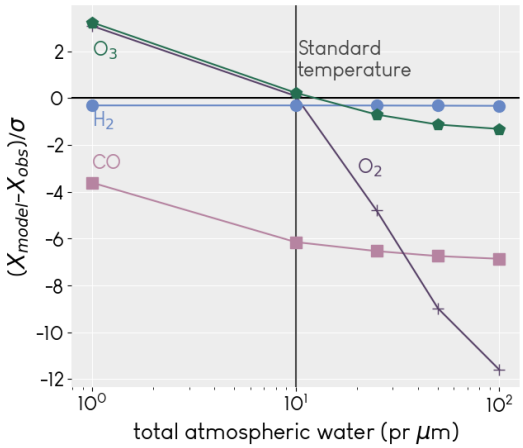

Figure 10. The same as Figure 9, but for model runs where we varied the water vapor content of the atmosphere.

GEL) requires an escape rate of approximately 3×10^9 cm^{-2} s^{-1}, an order of magnitude higher than what we currently observe for escape rates of H from Mars (Jakosky et al., 2018) and find in our modeling, in which $\phi_+\phi_D = 2\phi_O$. This is an indication that escape rates were likely higher in the past due to a variety of factors, especially in the context of a more UV-active young sun (Jakosky et al., 2018), or that surface interactions play a larger role that has not yet been fully quantified.

As a way to gain insight about our results, we compared the concentrations of a few molecular species in our model with available measurements (Figures 9 and 10). The measurements we used were the inferred lower atmospheric abundance of H_2 $= 15 \pm 5$ ppm (V. A. Krasnopolsky & Feldman, 2001); a global mean O_3 abundance of 1.2 μm-atm, extracted from maps by Clancy et al. (2016); and mixing ratios for O_2 and CO at the surface equal to $(5.8 \pm 0.8) \times 10^{-4}$ and $(1.61 \pm 0.09) \times 10^{-3}$ (Trainer et al., 2019). These comparisons indicate the model conditions which may be more similar or dissimilar to the current state of Mars. As one example, model results that used a particularly low temperature as input (for example, models with $T_{surf} < 190$ or $T_{exo} < 175$) diverge greatly from measurements of all molecular species. These model results thus represent a significant perturbation to the photochemical system as compared to modern

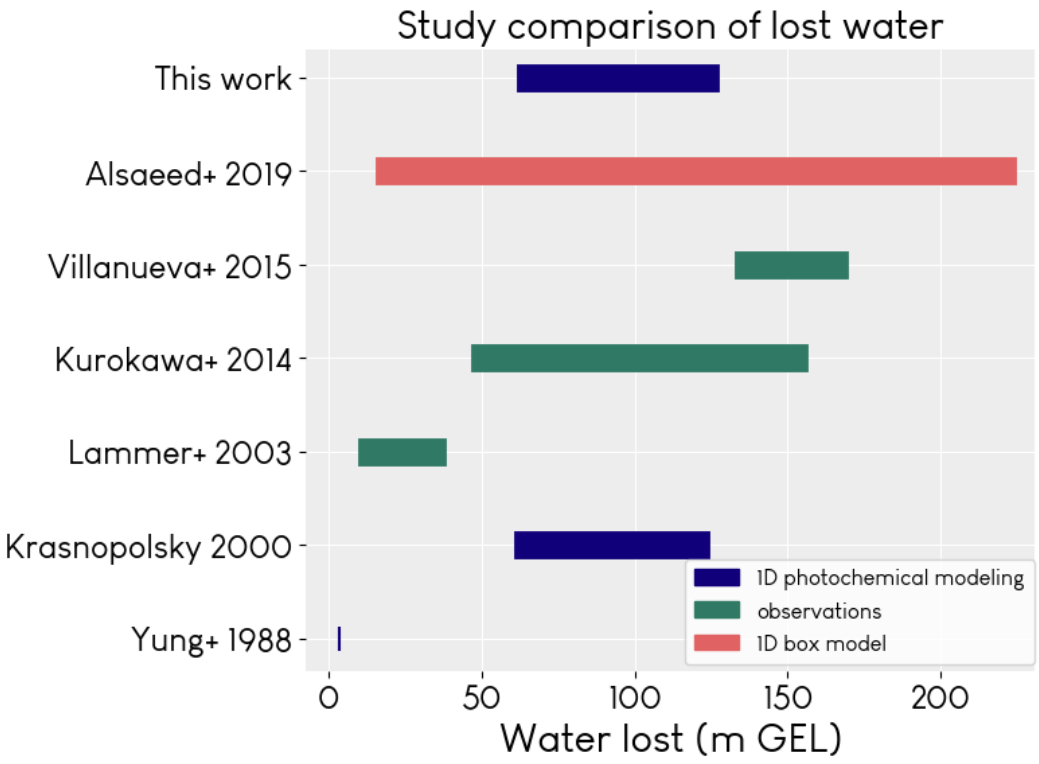

Figure 11. Estimates of water lost from Mars by various studies.

Mars. It is also important to note that O_3 and O_2 are related, as O_3 is created and destroyed via interactions between O_2 and O. CO sticks out as an obvious problem; this is not surprising, as many photochemical models also have difficulty in reproducing the observed values (V. A. Krasnopolsky, 2010). Some models come close (e.g. Zahnle et al. (2008)), usually only when another parameter changes significantly. Our model also underestimates CO, reaffirming the ongoing need for study in this area. Apart from CO, the difference between our model and measurements is mostly small, indicating that the standard atmosphere we chose was reasonable.

5 Conclusions

Our results in Figure 4 and Table S5 show that if only thermal escape isconsidered, D is almost completely retained on Mars compared to H. This is especially true near solar maximum, when most atmospheric escape overall occurs as thermal escape of H. During solar mean and minimum, however, thermal escape of H is low, and the fact that non-thermal escape dominates loss of D and HD (V. A. Krasnopolsky & Mumma, 1998; Gacesa et al., 2012) becomes much more significant. Our analysis show that including non-thermal escape significantly increases f by an order of magnitude or more for all atmospheric conditions, and that the tropopause temperature is the parameter with the greatest effect on f (Figure 4). Studies of only thermal escape are therefore not likely to provide a reasonable estimate of f. It is unclear whether the tropopause temperature's importance relates to a real, yet unknown, physical phenomenon, or whether it is an artifact resulting from our estimation of non-thermal escape. More modeling including non-thermal escape and observations of mesospheric phenomena are necessary to understand this effect in detail.

In reality, our results represent a peri-modern global scenario; f has likely changed over time in ways that our model does not account for. In this work, we consider only the exchangeable reservoirs of water on Mars without including any type of surface deposition, which comprises multiple processes with potentially different fractionation factors. Fractionation may also vary on seasonal timescales, especially around the poles, as HDO preferentially condenses and may also have a different sublimation rate compared to H_2O. It has certainly varied over geological time scales. We run the model for 10 million years to equilibrium, though it would not necessarily have been in equilibrium throughout its 4.5 billion year history. This also means that atmospheric escape rates would not have been constant in time. We assume escape rates to space to be constant because their time evolution is unknown. Mars' chaotically evolving obliquity on time scales greater than 10 million years is a major reason for this lack of a definitive paleoclimate timeline. Characterization of escape rates through time is therefore a critical, but daunting, subject for future modeling efforts. On early Mars, f would also have been different due to the more UV-active young sun, which would have enhanced non-thermal escape rates (Jakosky et al., 2018). For all these reasons, we expect that our results for water loss are a lower bound.

Future work to understand the fractionation factor and atmospheric escape will need to link cross-disciplinary knowledge of surface and atmospheric processes. The history of water on Mars cannot be fully understood by only considering one or the other; they are inextricably linked. A more thorough understanding of exchange between different water reservoirs on and under the surface and in the atmosphere, as well as the variables affecting all types of atmospheric escape and water loss, will be instrumental in forming a more complete picture of the fractionation factor, and by extension water loss, on Mars.

Acknowledgments

This work was supported by MDAP grant #NNX14AM20G. Additionally, this material is based upon work supported by the National Science Foundation Graduate Research Fellowship Program under Grant No. DGE 1650115. Any opinions, findings, and conclusions or recommendations expressed in this material are those of the author(s) and do not necessarily reflect the views of the National Science Foundation. The authors would like to thank B. Jakosky, N. Alsaeed, L. Wernicke, and D. Brain for ongoing collaboration, feedback, and support. The model, information necessary to construct inputs, and generated output can be found on the lead author's GitHub account at `https://github.com/emcangi/dh_fractionation`.

References

Anderson, D. E., & Hord, C. W. (1971). Mariner 6 and 7 Ultraviolet Spectrometer Experiment: Analysis of hydrogen Lyman-alpha data. *Journal of Geophysical Research*, *76*. doi: 10.1029/ja076i028p06666

Audouard, J., Piqueux, S., Poulet, F., Vincendon, M., Gondet, B., & Rogers, D. A. (2016). Analysis of Curiosity Surface Temperature Data. In *47th lunar and planetary sciences conference.*

Bertaux, J., & Montmessin, F. (2001). Isotopic fractionation through water vapor condensation: The Deuteropause, a cold trap for deuterium in the atmosphere of Mars. *Journal of Geophysical Research-Planets*, *106*. doi: 10.1029/2000JE001358

Bjoraker, G. L., Mumma, M. J., & Larson, H. P. (1989). Isotopic Abundance Ratios for Hydrogen and Oxygen in the Martian Atmosphere. In *AAS/Division for Planetary Sciences 21st annual meeting.*

Bougher, S. W., Roeten, K. J., Olsen, K., Mahaffy, P. R., Benna, M., Elrod, M., ... Jakosky, B. M. (2017). The structure and variability of Mars dayside

thermosphere from MAVEN NGIMS and IUVS measurements: Seasonal and solar activity trends in scale heights and temperatures. *Journal of Geophysical Research: Space Physics*, *122*. doi: 10.1002/2016JA023454

Carr, M., & Head, J. (2019). Mars: Formation and fate of a frozen Hesperian ocean. *Icarus*, *319*. doi: 10.1016/j.icarus.2018.08.021

Carr, M. H., & Head, J. W. (2010). Geologic history of Mars. *Earth and Planetary Science Letters*, *294*. doi: 10.1016/j.epsl.2009.06.042

Cazaux, S., Cobut, V., Marseille, M., Spaans, M., & Caselli, P. (2010). Water formation on bare grains: When the chemistry on dust impacts interstellar gas. *Astronomy & Astrophysics*, *522*. doi: 10.1051/0004-6361/201014026

Chaffin, M. S., Deighan, J., Schneider, N. M., & Stewart, A. I. F. (2017). Elevated atmospheric escape of atomic hydrogen from Mars induced by high-altitude water. *Nature Geoscience*, *10*. doi: 10.1038/ngeo2887

Clancy, R. T., Wolff, M. J., Lefèvre, F., Cantor, B. A., Malin, M. C., & Smith, M. D. (2016). Daily global mapping of Mars ozone column abundances with MARCI UV band imaging. *Icarus*, *266*. doi: 10.1016/j.icarus.2015.11.016

Clarke, J. T., Mayyasi, M., Bhattacharyya, D., et al. (2017). Variability of D and H in the Martian upper atmosphere observed with the MAVEN IUVS echelle channel. *Journal of Geophysical Research: Space Physics*, *122*. doi: 10.1002/2016JA023479

Clarke, J. T., Mayyasi, M., Bhattacharyya, D., Schneider, N., Chaufray, J.-Y., Bertaux, J.-L., ... Yelle, R. (2019, Sept). The D/H Ratio in the Martian Upper Atmosphere. In *European Planetary Science Congress and AAS/Division for Planetary Sciences 2019 joint meeting.* (EPSC-DPS2019-868-1)

Deighan, J. (2012). *The effect of an ozone layer on ancient mars* (Doctoral dissertation, University of Virginia). Retrieved from `http://libra.virginia.edu/catalog/libra-oa:2577`

Ehlmann, B. L., & Edwards, C. S. (2014). Mineralogy of the Martian Surface. *Annual Review of Earth and Planetary Sciences*, *42*. doi: 10.1146/annurev-earth-060313-055024

Encrenaz, T., DeWitt, C., Richter, M. J., Greathouse, T. K., Fouchet, T., Montmessin, F., ... Sagawa, H. (2018). New measurements of D/H on Mars using EXES aboard SOFIA. *Astronomy & Astrophysics*, *612*. doi: 10.1051/0004-6361/201732367

Fedorova, A. A., Montmessin, F., Korablev, O., Luginin, M., Trokhimovsky, A., Belyaev, D. A., ... Wilson, C. F. (2020). Stormy water on Mars: the behavior and saturation of atmospheric water during the dusty season. *Submitted to Science*, *9522*. doi: 10.1126/science.aay9522

Fouchet, T., & Lellouch, E. (1999). Vapor Pressure Isotope Fractionation Effects in Planetary Atmospheres: Application to Deuterium. *Icarus*, *144*. doi: 10.1006/icar.1999.6264

Gacesa, M., Zhang, P., & Kharchenko, V. (2012). Non-thermal escape of molecular hydrogen from Mars. *Geophysical Research Letters*, *39*. doi: 10.1029/2012GL050904

Geiss, J., & Reeves, H. (1981). Deuterium in the solar system. *Astronomy & Astrophysics*, *93*.

Heavens, N. G., Kleinböhl, A., Chaffin, M. S., et al. (2018). Hydrogen escape from Mars enhanced by deep convection in dust storms. *Nature Astronomy*, *2*. doi: 10.1038/s41550-017-0353-4

Hunten, D. M. (1973). The Escape of Light Gases from Planetary Atmospheres. *Journal of the Atmospheric Sciences*, *30*. doi: 10.1016/0032-0633(82)90110-6

Jakosky, B. M., Brain, D. A., Chaffin, M. S., et al. (2018). Loss of the Martian atmosphere to space: Present-day loss rates determined from MAVEN observations and integrated loss through time. *Icarus*. doi: 10.1016/j.icarus.2018.05.030

Klingelhöfer, G., Morris, R. V., Bernhardt, B., Schröder, C., Rodionov, D. S., de Souza, P. A., ... Arvidson, R. E. (2004). Jarosite and Hematite at Meridiani Planum from Opportunity's Mössbauer Spectrometer. *Science*, *306*. doi: 10.1126/science.1104653

Krasnopolsky, V. (1993). Photochemistry of the Martian Atmosphere (Mean Conditions). *Icarus*, *101*. doi: 10.1006/icar.1993.1027

Krasnopolsky, V. (2000). On the Deuterium Abundance on Mars and Some Related Problems. *Icarus*, *148*. doi: 10.1006/icar.2000.6534

Krasnopolsky, V., Bjoraker, G., Mumma, M., & Jennings, D. (1997). High-resolution spectroscopy of Mars at 3.7 and 8 μm:A sensitive search for H2O2, H2CO, HCI, and CH4, and detection of HDO. *Journal of Geophysical Research*, *102*. doi: 10.1029/96JE03766

Krasnopolsky, V. A. (2002). Mars' upper atmosphere and ionosphere at low, medium, and high solar activities: Implications for evolution of water. *Journal of Geophysical Research: Planets*, *107*. doi: 10.1029/2001JE001809

Krasnopolsky, V. A. (2010). Solar activity variations of thermospheric temperatures on Mars and a problem of CO in the lower atmosphere. *Icarus*, *207*. doi: 10.1016/j.icarus.2009.12.036

Krasnopolsky, V. A., & Feldman, P. D. (2001). Detection of molecular hydrogen in the atmosphere of Mars. *Science*, *294*. doi: 10.1126/science.1065569

Krasnopolsky, V. A., & Mumma, M. J. (1998). Detection of Atomic Deuterium in the Upper Atmosphere of Mars. *Science*, *280*. doi: 10.1126/science.280.5369.1576

Lammer, H., Kolb, C., Penz, T., Amerstorfer, U. V., Biernat, H. K., & Bodiselitsch, B. (2003). Estimation of the past and present Martian water-ice reservoirs by isotopic constraints on exchange between the atmosphere and the surface. *International Journal of Astrobiology*, *2*. doi: 10.1017/S1473550403001605

Laskar, J., Correia, A., Gastineau, M., Joutel, F., Levrard, B., & Robutel, P. (2004). Long term evolution and chaotic diffusion of the insolation quantities of Mars. *Icarus*, *170*. doi: 10.1016/J.ICARUS.2004.04.005

Lasue, J., Mangold, N., Hauber, E., et al. (2013). Quantitative Assessments of the Martian Hydrosphere. *Space Science Reviews*, *174*. doi: 10.1007/s11214-012-9946-5

Mahaffy, P. R., Webster, C. R., Stern, J. C., Brunner, A. E., Atreya, S. K., Conrad, P. G., ... Wray, J. J. (2015). The imprint of atmospheric evolution in the D/H of hesperian clay minerals on Mars. *Science*, *347*. doi: 10.1126/science.1260291

Maltagliati, L. (2011). Evidence of Water Vapor in Excess of Saturation in the Atmosphere of Mars. *Science*, *333*. doi: 10.1126/science.1207957

Manion, J. A., Huie, R. E., Levin, R. D., Burgess Jr., D. R., Orkin, V. L., Tsang, W., ... Frizzell, D. H. (2015). *NIST Chemical Kinetics Database.* Retrieved 2015-09, from `http://kinetics.nist.gov/`

Marti, J., & Mauersberger, K. (1993). A Survey and New Measurements of Ice Vapor Pressure at Temperatures Between 170 and 250K. *Geophysical Research Letters*, *20*. doi: 10.1029/93GL00105

Matta, M., Withers, P., & Mendillo, M. (2013). The composition of Mars' topside ionosphere: Effects of hydrogen. *Journal of Geophysical Research: Space Physics*, *118*. doi: 10.1002/jgra.50104

McElroy, D., Walsh, C., Markwick, A. J., Cordiner, M. A., Smith, K., & Millar, T. J. (2013). *The UMIST database for Astrochemistry 2012.*

Millour, E., & Forget, F. (2018). *Mars Climate Database.* Retrieved from `http://www-mars.lmd.jussieu.fr/`

Montmessin, F., Fouchet, T., & Forget, F. (2005). Modeling the annual cycle of HDO in the Martian atmosphere. *Journal of Geophysical Research E: Planets*, *110*. doi: 10.1029/2004JE002357

Nair, H., Allen, M., Anbar, A. D., & Yung, Y. L. (1994). A Photochemical Model of the Martian Atmosphere. *Icarus*, *111*. doi: 10.1006/icar.1994.1137

Owen, T., Maillard, J. P., de Bergh, C., & Lutz, B. L. (1988). Deuterium on Mars: The Abundance of HDO and the Value of D/H. *Science (New York, N.Y.)*, *240*. doi: 10.1126/science.240.4860.1767

Ramirez, R. M., Kopparapu, R., Zugger, M. E., Robinson, T. D., Freedman, R., & Kasting, J. F. (2014). Warming early Mars with CO2 and H2. *Nature Geoscience*, *7*. doi: 10.1038/ngeo2000

Sander, S. P., Friedl, R. R., Golden, D. M., Kurylo, M. J., Moortgat, G. K., Wine, P. H., ... Orkin, V. L. (2011). Chemical Kinetics and Photochemical Data for Use in Atmospheric Studies Evaluation Number 15. *Cross Sections*. doi: 10.1002/kin.550171010

Savijärvi, H., McConnochie, T. H., Harri, A. M., & Paton, M. (2019). Water vapor mixing ratios and air temperatures for three martian years from Curiosity. *Icarus*, *326*. doi: 10.1016/j.icarus.2019.03.020

Shaposhnikov, D. S., Medvedev, A. S., Rodin, A. V., & Hartogh, P. (2019). Seasonal Water "Pump" in the Atmosphere of Mars: Vertical Transport to the Thermosphere. *Geophysical Research Letters*, *46*. doi: 10.1029/2019GL082839

Smith, M. D. (2004). Interannual variability in TES atmospheric observations of Mars during 1999-2003. *Icarus*, *167*. doi: 10.1016/j.icarus.2003.09.010

Smith, M. D., Wolff, M. J., Spanovich, N., Ghosh, A., Banfield, D., Christensen, P. R., ... Squyres, S. W. (2006). One Martian year of atmospheric observations using MER Mini-TES. *Journal of Geophysical Research E: Planets*, *111*. doi: 10.1029/2006JE002770

Squyres, S. W., Grotzinger, J. P., Arvidson, R. E., Bell, J. F., Calvin, W., Christensen, P. R., ... Soderblom, L. A. (2004). In Situ Evidence for an Ancient Aqueous Environment at Meridiani Planum, Mars. *Science*, *306*. doi: 10.1126/science.1104559

Stone, S. W., Yelle, R. V., Benna, M., Elrod, M. K., & Mahaffy, P. R. (2018). Thermal Structure of the Martian Upper Atmosphere From MAVEN NGIMS. *Journal of Geophysical Research: Planets*. doi: 10.1029/2018JE005559

Thiemann, E. M. B., Eparvier, F. G., Bougher, S. W., Dominique, M., Andersson, L., Girazian, Z., ... Jakosky, B. M. (2018). Mars Thermospheric Variability Revealed by MAVEN EUVM Solar Occultations: Structure at Aphelion and Perihelion and Response to EUV Forcing. *Journal of Geophysical Research (Planets)*, *123*. doi: 10.1029/2018JE005550

Trainer, M. G., Wong, M. H., McConnochie, T. H., Franz, H. B., Atreya, S. K., Conrad, P. G., ... Zorzano, M. P. (2019). Seasonal Variations in Atmospheric Composition as Measured in Gale Crater, Mars. *Journal of Geophysical Research: Planets*, *124*. doi: 10.1029/2019JE006175

Usui, T., Alexander, C. M. O., Wang, J., Simon, J. I., & Jones, J. H. (2012). Evidence from Olivine-Hosted Melt Inclusions that the Martian Mantle has a Chondritic D/H Ratio and that Some Young Basalts have Assimilated Old Crust. In *Lunar and planetary science conference.*

Vandaele, A. C., Korablev, O., Daerden, F., Aoki, S., Thomas, I. R., Altieri, F., ... others (2019). Martian dust storm impact on atmospheric H 2 O and D/H observed by ExoMars Trace Gas Orbiter. *Nature*, *568*. doi: 10.1038/s41586-019-1097-3

Vasavada, A. R., Piqueux, S., Lewis, K. W., Lemmon, M. T., & Smith, M. D. (2016). Thermophysical properties along Curiosity's traverse in Gale crater, Mars, derived from the REMS ground temperature sensor. *Icarus*, *284*. doi: 10.1016/j.icarus.2016.11.035

Villanueva, G. L., Liuzzi, G., Crismani, M. M., et al. (2019). Strong seasonal and diurnal variabilityof water D/H on Marsas revealed with ExoMars/NOMAD. In *Epsc abstracts.* (EPSC-DPS2019-1471)

Villanueva, G. L., Mumma, M. J., Novak, R. E., et al. (2015). Strong water isotopic anomalies in the martian atmosphere: Probing current and ancient reservoirs. *Science*, *348*. doi: 10.1126/science.aaa3630

Wakelam, V., & Gratier, P. (2019). *Kinetic Database for Astrochemistry.* Retrieved from `http://kida.obs.u-bordeaux1.fr/contact.html`

Woods, T. N., Chamberlin, P. C., Harder, J. W., Hock, R. A., Snow, M., Eparvier, F. G., ... Richard, E. C. (2019). *LISIRD (LASP Interactive Solar Irradiance Datacenter).* Retrieved from `http://lasp.colorado.edu/lisird/`

Wordsworth, R., Kalugina, Y., Lokshtanov, S., Vigasin, A., Ehlmann, B., Head, J., ... Wang, H. (2017, March). Transient Reducing Atmospheres on Early Mars as a Solution to the Faint Young Sun Paradox. In *Lunar and planetary science conference.*

Wordsworth, R. D., Kerber, L., Pierrehumbert, R. T., Forget, F., & Head, J. W. (2015). Comparison of "warm and wet" and "cold and icy" scenarios for early Mars in a 3D climate model. *Journal of Geophysical Research: Planets*. doi: 10.1002/2015JE004787

Yung, Y. L., & DeMore, W. B. (1998). *Photochemistry of Planetary Atmospheres.* Oxford University Press.

Yung, Y. L., Wen, J.-S., Moses, J. I., Landry, B. M., Allen, M., & Hsu, K.-J. (1989). Hydrogen and deuterium loss from the terrestrial atmosphere: A quantitative assessment of nonthermal escape fluxes. *Journal of Geophysical Research*, *94*.

Yung, Y. L., Wen, J. S., Pinto, J. P., Allen, M., Pierce, K. K., & Paulson, S. (1988). HDO in the Martian atmosphere: Implications for the abundance of crustal water. *Icarus*, *76*. doi: 10.1016/0019-1035(88)90147-9

Zahnle, K., Haberle, R. M., Catling, D. C., & Kasting, J. F. (2008). Photochemical instability of the ancient Martian atmosphere. *Journal of Geophysical Research E: Planets*, *113*. doi: 10.1029/2008JE003160

Figure 1.

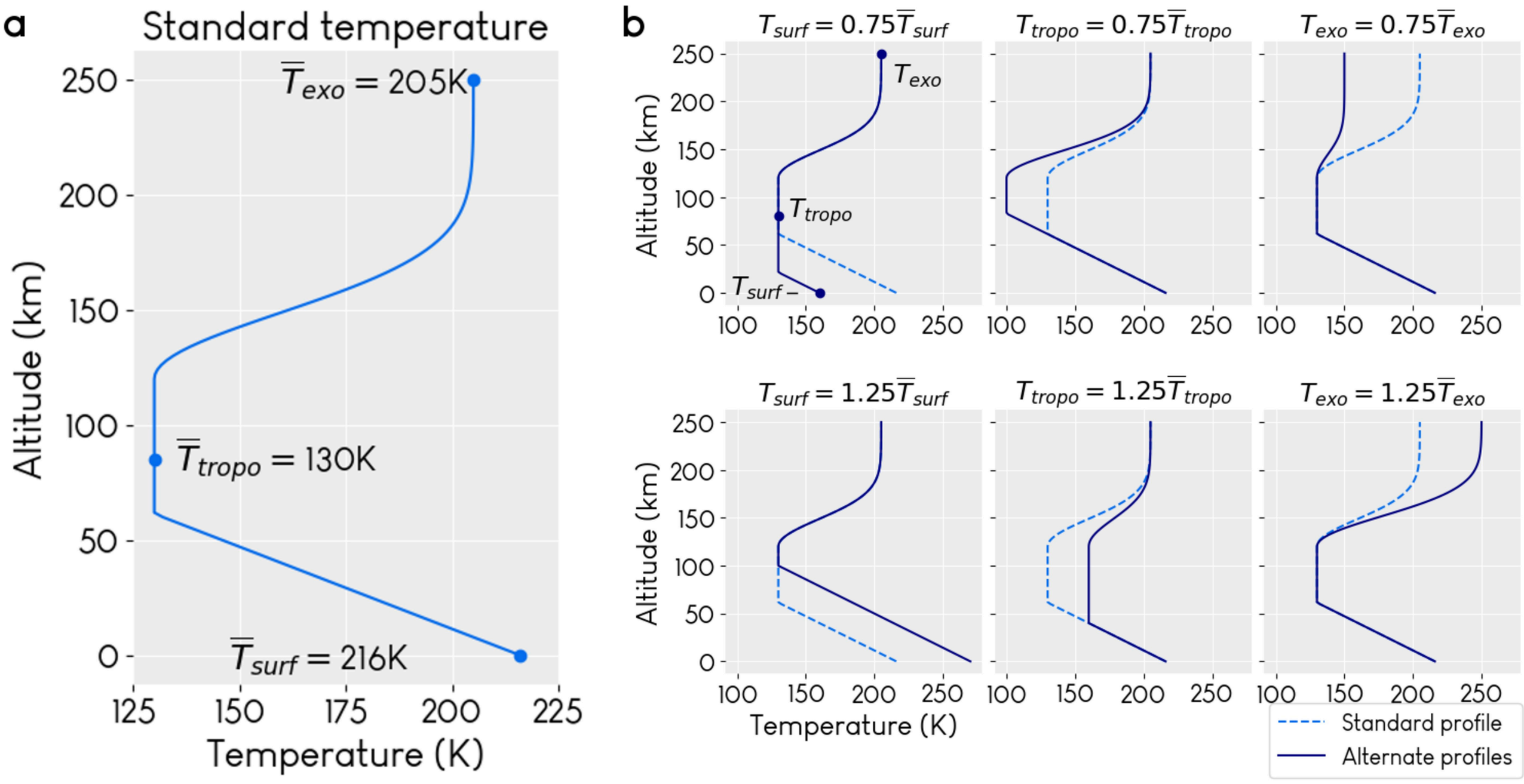
a
Standard temperature
$\overline{T}_{exo} = 205K$
$\overline{T}_{tropo} = 130K$
$\overline{T}_{surf} = 216K$
Altitude (km)
Temperature (K)
b
$T_{surf} = 0.75\overline{T}_{surf}$
$T_{tropo} = 0.75\overline{T}_{tropo}$
$T_{exo} = 0.75\overline{T}_{exo}$
$T_{surf} = 1.25\overline{T}_{surf}$
$T_{tropo} = 1.25\overline{T}_{tropo}$
$T_{exo} = 1.25\overline{T}_{exo}$
T_{exo}
T_{tropo}
T_{surf}
Standard profile
Alternate profiles

Figure 2.

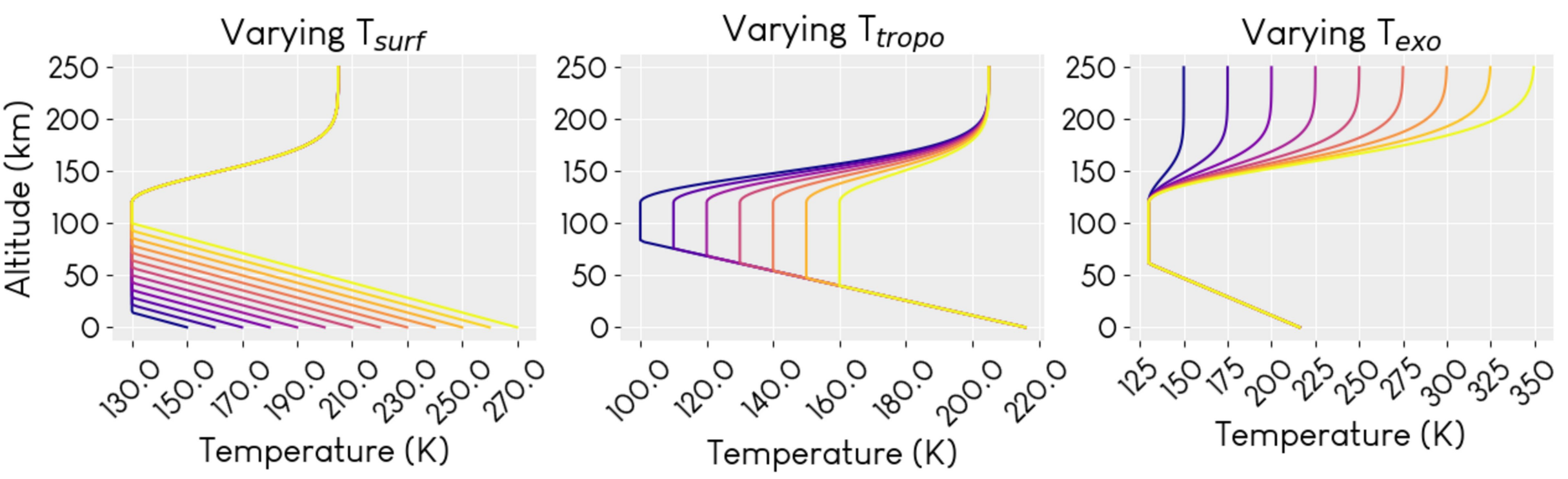
Varying T_{surf}
Varying T_{tropo}
Varying T_{exo}
Altitude (km)
0
50
100
150
200
250
130.0
150.0
170.0
190.0
210.0
230.0
250.0
270.0
100.0
120.0
140.0
160.0
180.0
200.0
220.0
125
150
175
200
225
250
275
300
325
350
Temperature (K)
Temperature (K)
Temperature (K)

Figure 3.

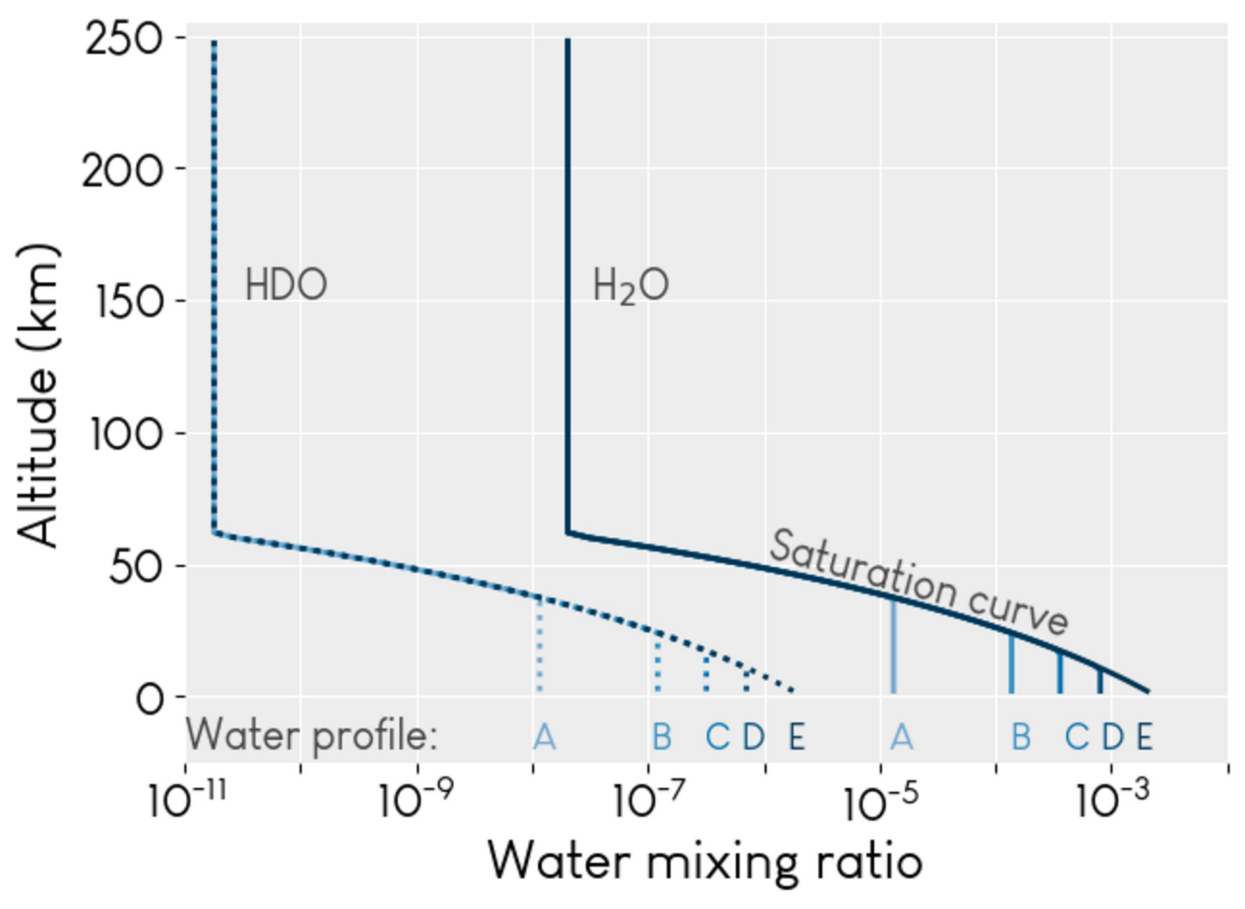
250
200
150
100
50
0
Altitude (km)
HDO
H2O
Saturation curve
Water profile:
A
B
C
D
E
A
B
C
D
E
10-11
10-9
10-7
10-5
10-3
Water mixing ratio

Figure 4.

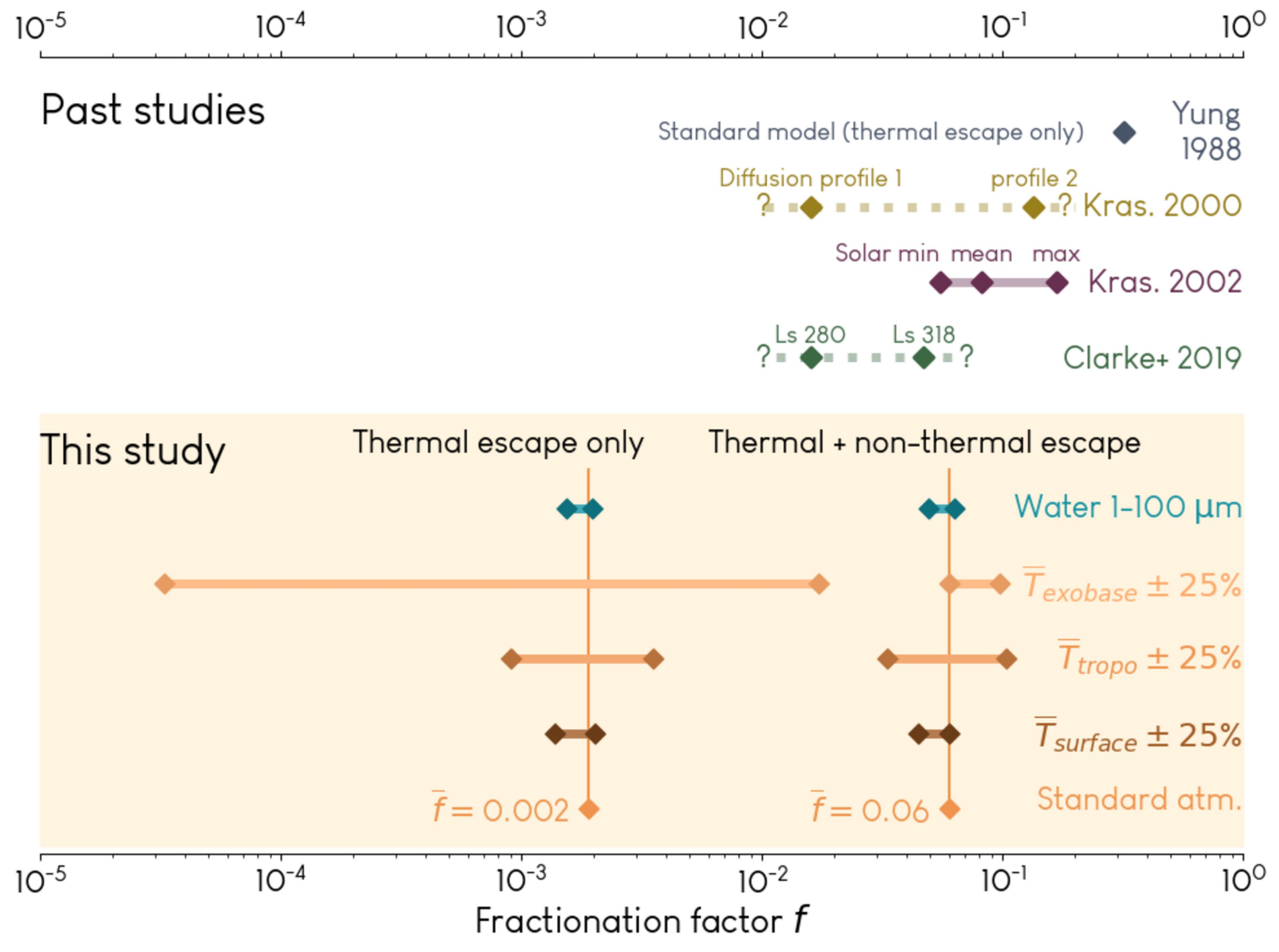
10-5
10-4
10-3
10-2
10-1
100
Past studies
Standard model (thermal escape only)
Yung 1988
Diffusion profile 1
profile 2
?
?
Kras. 2000
Solar min
mean
max
Kras. 2002
Ls 280
Ls 318
?
?
Clarke+ 2019
This study
Thermal escape only
Thermal + non-thermal escape
Water 1-100 µm
$\overline{T}_{exobase}$ ± 25%
$\overline{T}_{tropo}$ ± 25%
$\overline{T}_{surface}$ ± 25%
Standard atm.
$\bar{f}$ = 0.002
$\bar{f}$ = 0.06
10-5
10-4
10-3
10-2
10-1
100
Fractionation factor f

Figure 5.

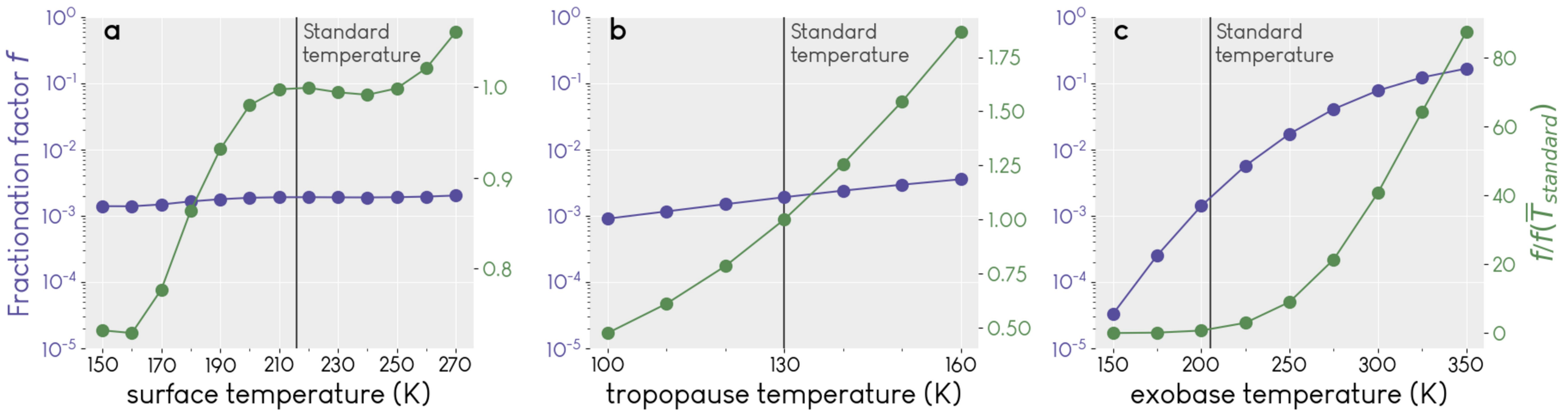
a
Standard temperature
Fractionation factor f
surface temperature (K)
b
Standard temperature
tropopause temperature (K)
c
Standard temperature
exobase temperature (K)
f/f(T̄ standard)

Figure 6.

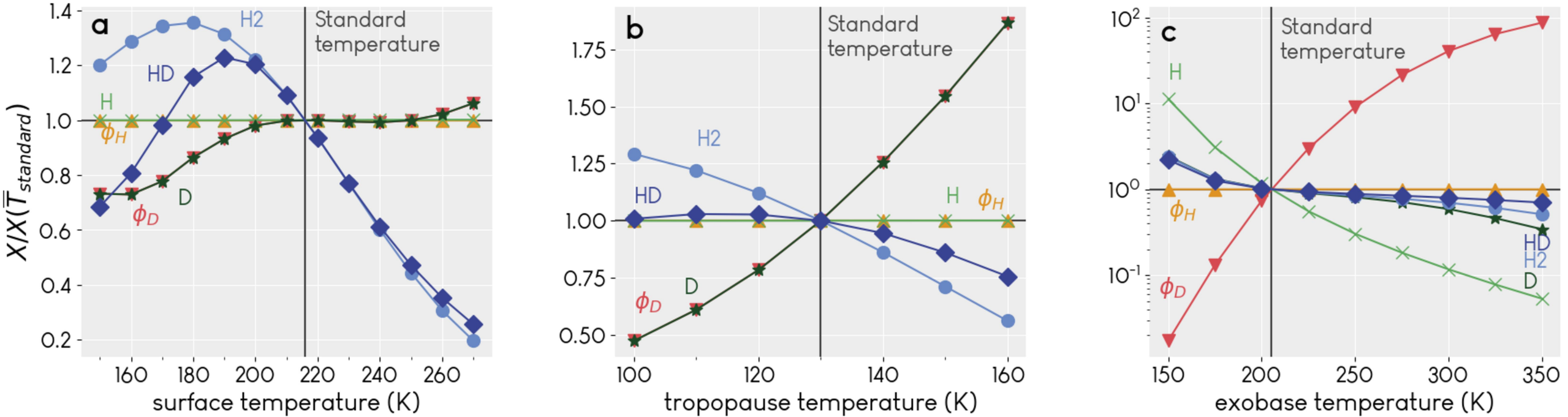
a
b
c
Standard temperature
H2
HD
H
D
ϕ_H
ϕ_D
$X/X(\overline{T}_{standard})$
surface temperature (K)
tropopause temperature (K)
exobase temperature (K)

Figure 7.

a

Standard temperature

0.0020
0.0019
0.0018
0.0017
0.0016
0.0015

f

1.10
1.05
1.00
0.95
0.90
0.85
0.80

$f/f(\overline{T}_{standard})$

b

H_2

H

ϕ_H

ϕ_D

HD

D

1.05
1.00
0.95
0.90
0.85

$X/X(\overline{T}_{standard})$

Standard temperature

10^0
10^1
10^2

total atmospheric water (pr μm)

Figure 8.

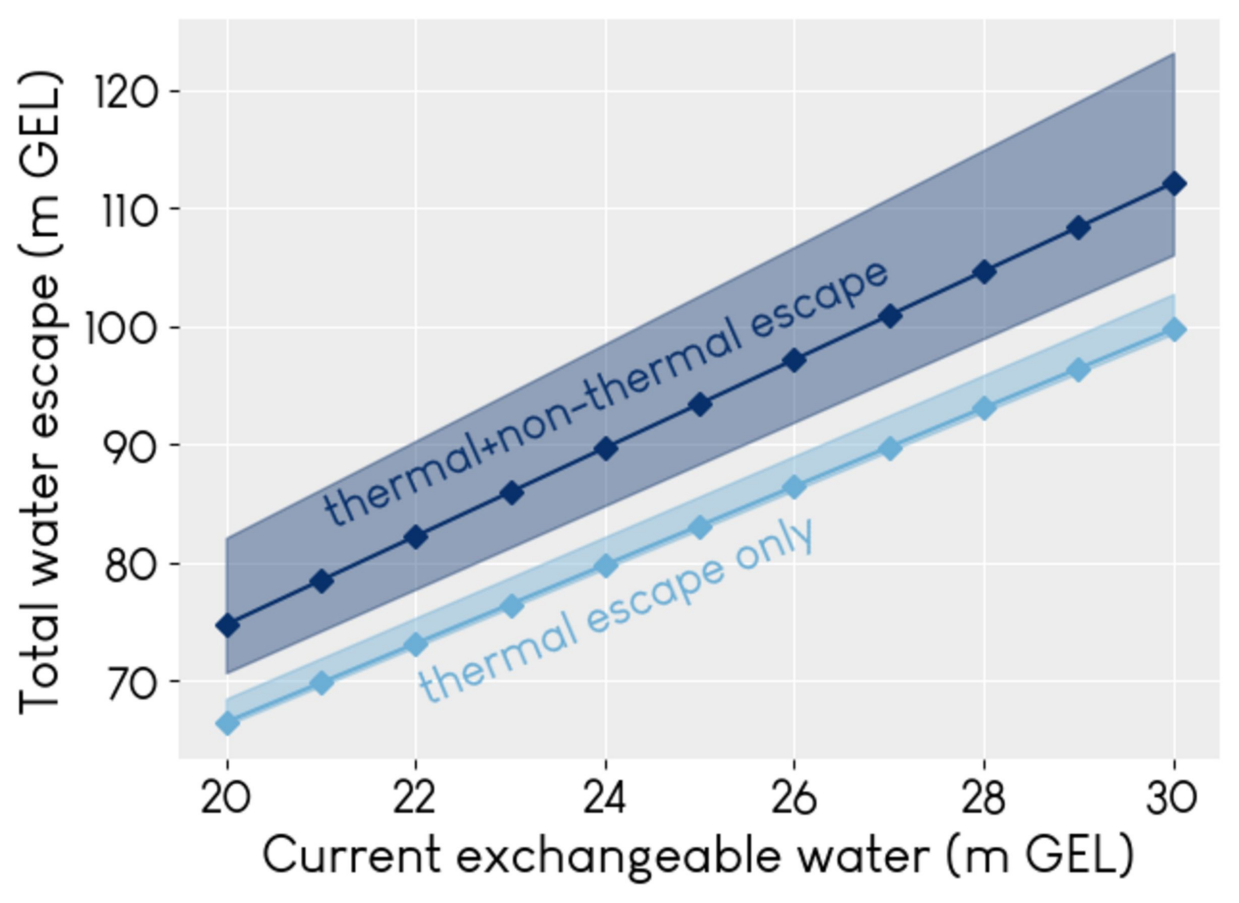
Total water escape (m GEL)
120
110
100
90
80
70
thermal+non-thermal escape
thermal escape only
20
22
24
26
28
30
Current exchangeable water (m GEL)

Figure 9.

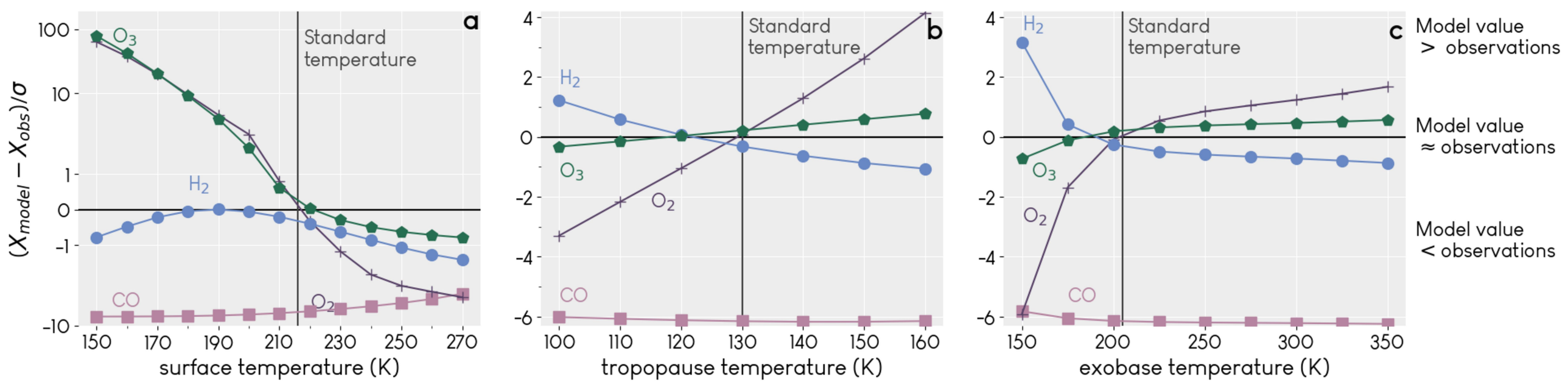
a
b
c
Standard temperature
$(X_{model} - X_{obs})/\sigma$
O_3
H_2
CO
O_2
surface temperature (K)
tropopause temperature (K)
exobase temperature (K)
Model value > observations
Model value ≈ observations
Model value < observations

Figure 10.

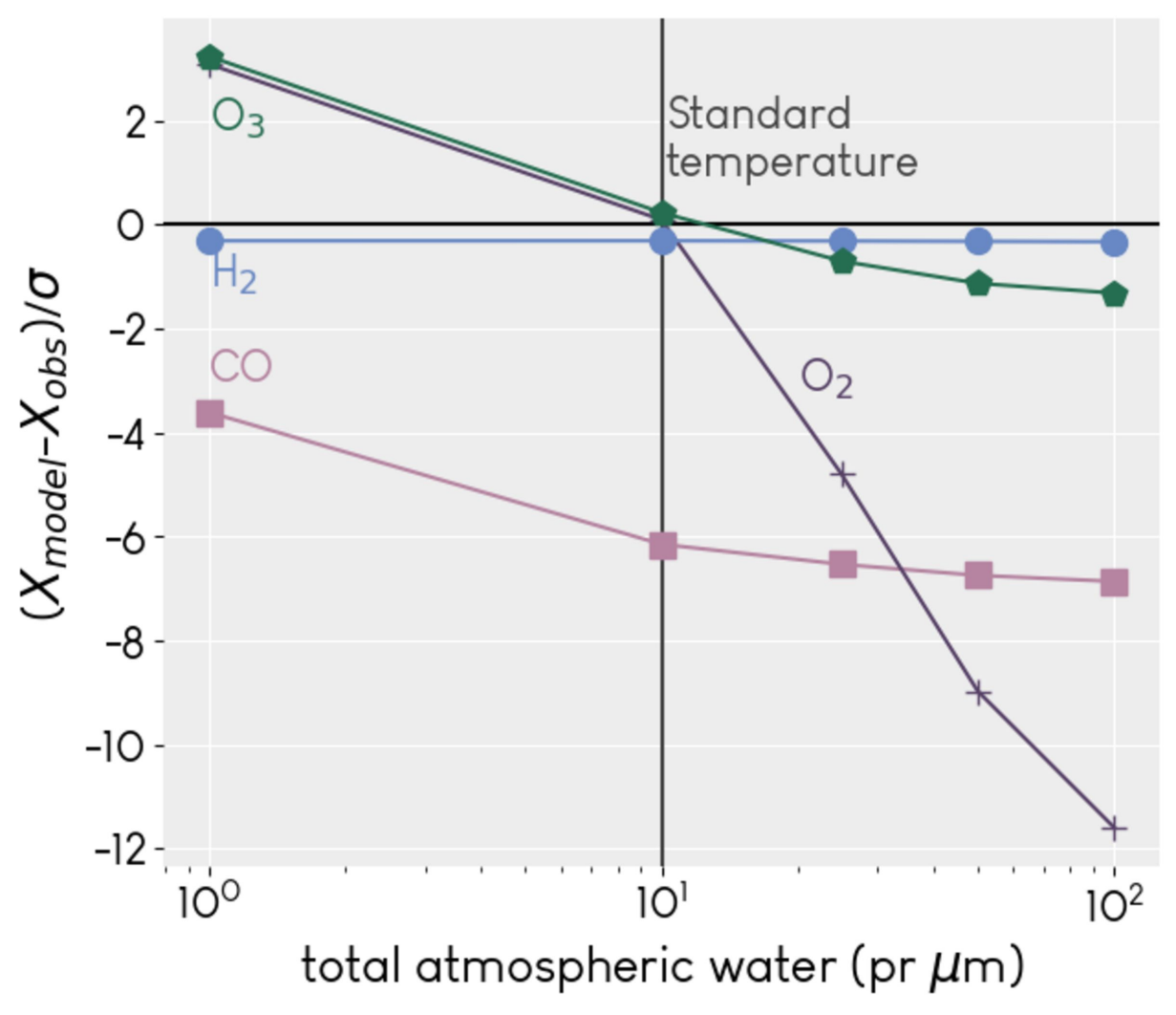
$(X_{model}-X_{obs})/\sigma$
2
0
-2
-4
-6
-8
-10
-12
O_3
H_2
CO
O_2
Standard
temperature
10^0
10^1
10^2
total atmospheric water (pr μm)

Figure 11.

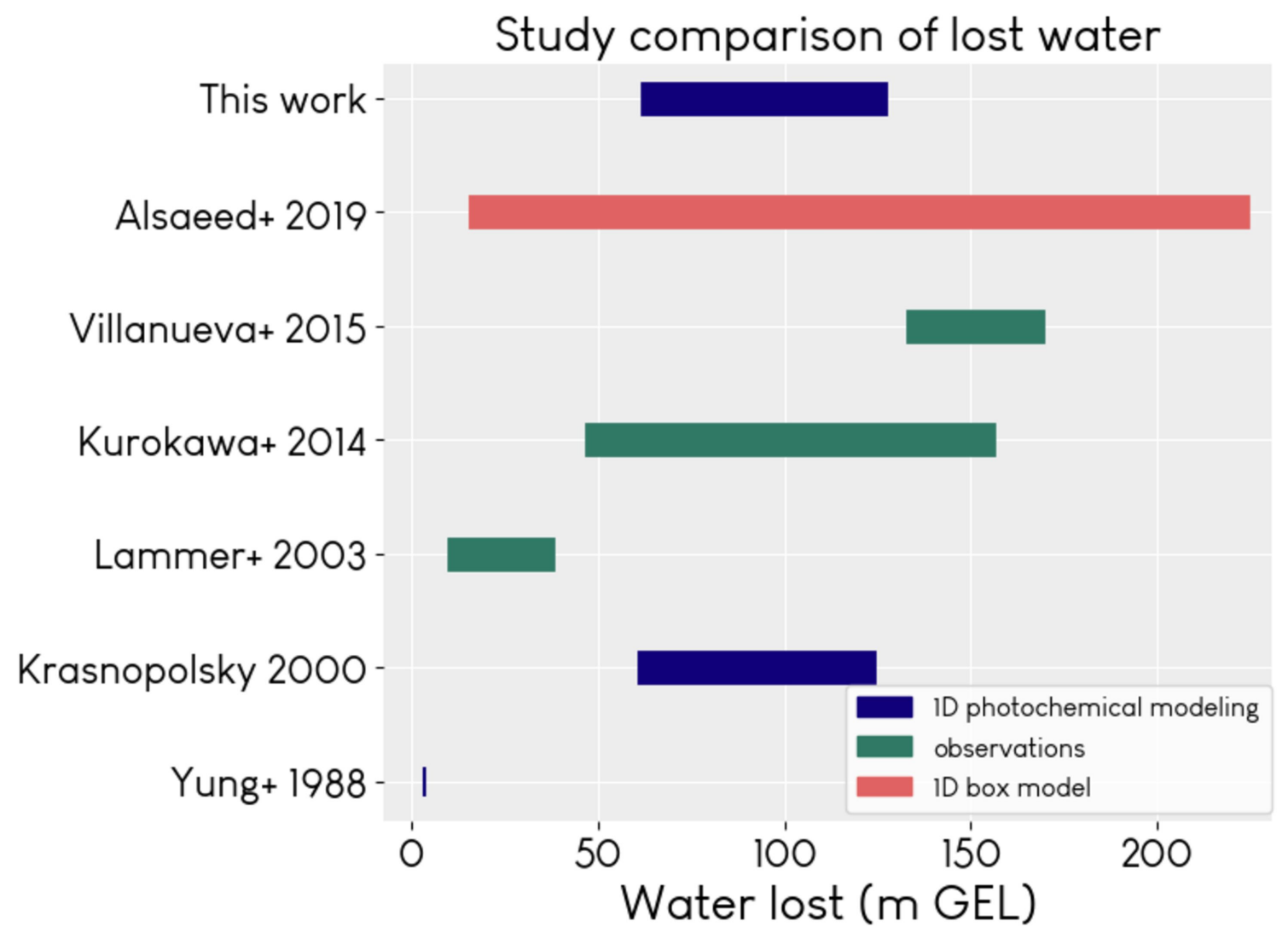
Study comparison of lost water
This work
Alsaeed+ 2019
Villanueva+ 2015
Kurokawa+ 2014
Lammer+ 2003
Krasnopolsky 2000
Yung+ 1988
1D photochemical modeling
observations
1D box model
0
50
100
150
200
Water lost (m GEL)